sustainability

MDPI

Article

Research on Bearing Capacity of Secant Piled-Bucket Foundation in Saturated Clay

Ying Xu [1,2], Haijun Wang [1,2,*], Liying Zhang [3], Mingji Deng [3], Hechuan Jiang [3], Yaohua Guo [1,2] and Xu Yang [1,2]

1 State Key Laboratory of Hydraulic Engineering Simulation and Safety, Tianjin University, Tianjin 300350, China
2 School of Civil Engineering, Tianjin University, Tianjin 300350, China
3 China Huaneng Group, Clean Energy Research Institute, Beijing 102209, China
* Correspondence: bookwhj@163.com

Abstract: The secant piled-bucket foundation (SPBF) is innovatively proposed to suit the large-capacity mainstream, which is optimized from a traditional foundation and consists of an upper pile cap and a lower bucket skirt. Compared with the pile foundation, the SPBF has great advantages and deserves further study. In this research, the bearing mode, bearing capacity and failure mode under various loads of SPBF in saturated clay have been fully studied. First, the small-scale model test in saturated clay is carried out to verify the finite element (FE) method; the deviation between the FE results and the test results under vertical load and horizontal–moment load is 10.65% and 10.25%, respectively. Next, the bearing mode of SPBF in engineering scales is investigated via FE method, the results indicating that the bearing mode of SPBF is similar to that of a prestressed tubular foundation. Finally, the bearing capacity and failure mode of SPBF are studied and the findings show that the vertical bearing capacity and horizontal–moment bearing capacity of SPBF is 96.53 MN and 1.62 MN, and the weak parts of SPBF are concrete of the pile cap and the anchor bolts, respectively. This paper provides support for design and further optimization in the future.

Keywords: bearing capacity; onshore wind; secant piled-bucket foundation; finite element analysis

check for updates

Citation: Xu, Y.; Wang, H.; Zhang, L.; Deng, M.; Jiang, H.; Guo, Y.; Yang, X. Research on Bearing Capacity of Secant Piled-Bucket Foundation in Saturated Clay. *Sustainability* **2022**, *14*, 11511. https://doi.org/10.3390/su141811511

Academic Editor: Francesco Granata

Received: 15 August 2022
Accepted: 8 September 2022
Published: 14 September 2022

1. Introduction

With the development of human civilization, greenhouse gas emissions, energy shortages and other issues have become increasingly prominent, and developing clean energy has become one of the ways to solve these issues. As a clean and environmentally friendly renewable energy, the onshore wind energy industry maintains rapid development and has gained a great share of the wind power market in recent decades, and the development of onshore wind energy has entered a mature stage and can be regarded as a promising industry [1].

Although onshore wind power has been well developed, there is still room for innovation. As the obvious developing trend of large-capacity wind turbines of the entire wind industry, the loads that transferred to the foundation during the operation continue to increase, resulting in the insufficient bearing capacity of the foundation, and a greater overturning failure probability of the existing traditional onshore wind turbine foundation. Therefore, in order to ensure the safety of wind turbines during operation, it is necessary to optimize the existing traditional foundation structures. Currently, the bucket foundation has become one of the most popular wind turbine foundation structure types and is widely used in offshore wind power projects due to the advantages of low cost, suitability for different geological conditions and convenient construction [2–6]. The innovative secant piled-bucket foundation (SPBF) for onshore wind turbines, which refers to the commercially applied offshore bucket foundation, can meet the entire market demand, and achieve the purpose of reducing cost and increasing efficiency [7].

The innovation SPBF is unique in structure and has certain advantages in construction cost. It is the first time that the secant pile support structure in municipal engineering is creatively applied to the wind power foundation. The SPBF consists of the upper (gravity) pile cap and lower (secant piled) bucket skirt. The lower bucket skirt is creatively composed of overlapping (secant) plain concrete piles and reinforced concrete piles, the detailed schematic is shown in Figure 1. At present, the first SPBF has been successfully applied to a 3.3 MW wind turbine in Jilin and has been connected to the grid for power generation. After a period of structural health monitoring, the results show that the onshore wind turbine with SPBF can operate safely. The project has proven that the SPBF could save approximately 40% of the land occupation, 22% of steel bars consumption, and 9% of concrete consumption compared with the 3.3 MW traditional onshore wind turbine foundation in the same wind farm (see Figure 2). It has been proved that SPBF will have great application prospects after structural optimization and production in the future. However, whether the SPBF has sufficient bearing capacity and safety margin, and what causes the foundation failure, is not clear, and needs further study.

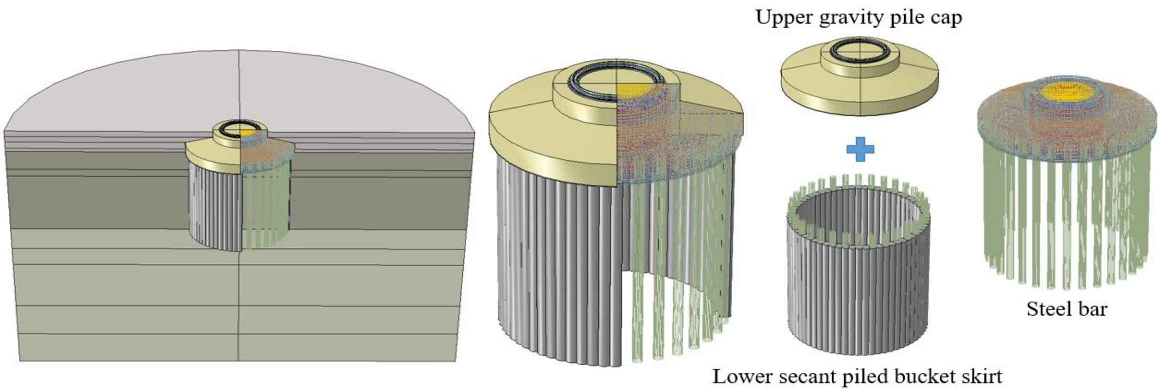

Figure 1. Diagram of secant piled-bucket foundation.

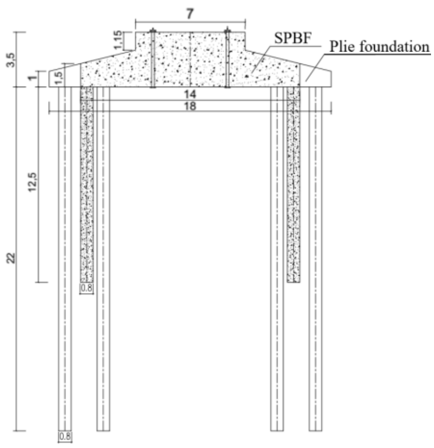

Figure 2. Comparison between SPBF and pile foundation (unit: m).

Since SPBF has the characteristics of a pile foundation and bucket foundation, the bearing mode of SPBF is unclear. The bearing mode of prestressed tubular foundation relies on the inner and outer earth pressure of the bucket skirt to resist the external force, while that of the pile foundation mainly relies on the side friction and tip resistance provided by the friction between piles and soil to resist external forces (see Figure 3). It is necessary to figure out whether the SPBF is analyzed according to the pile foundation or prestressed tubular foundation in the Code for Design of Wind Turbine Foundations for Onshore Wind Power Projects (NB/T 10311-2019) [8]. That will affect the choice of the bearing capacity calculation method of SPBF in the design stage.

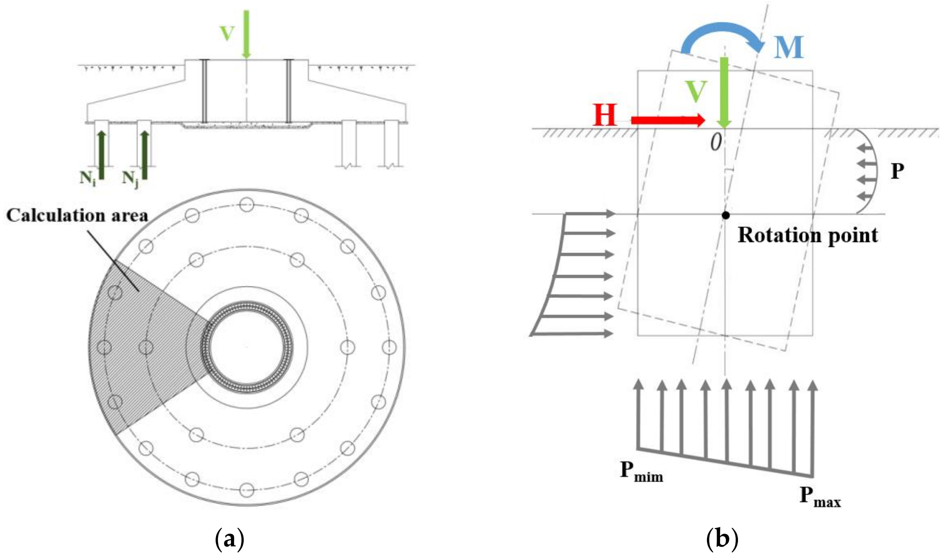

Figure 3. The bearing mode of foundation [8]. (**a**) Pile foundation. (**b**) Prestressed tubular foundation.

Experimentation is one of the most important research methods. The large-scale model test [6,9–12] and the field prototype test [13–16] can accurately simulate the stress state and performances of foundation structures but have huge economic costs and test sites, and are not suitable for the current stage of investigation. The small-scale model test [3,17–21] aims to draw regular conclusions, provide guidance to the design, and verify the finite element (FE) method and theoretical calculation, and has become the most widely used research method. Therefore, in this research, small-scale model tests are applied in the further research of SPBF.

However, the bearing capacity and failure mode of foundation in practical engineering cannot be observed intuitively through experimental phenomena. The appropriate finite element method can make up for the shortcomings in the small-scale model test. The FE method is widely used by scholars because of the characteristics of rapidity, economy, and repeatability, and can accurately reflect the complex soil–structure interaction, the bearing capacity and the failure mode of foundation in practical engineering [22–29]. However, the setting of boundary conditions, the selection of the mesh type and the division of the mesh of the model are all dependent on the existing experience, and it is not clear whether the current FE method is applicable to the study of SPBF. The applicability of these settings in the analysis of the innovation SPBF and the accuracy of the FE results obtained based on these settings still need further verification for subsequent research.

The SPBF has good economics and great application prospects, but whether there is still room for further optimization of SPBF needs to be clarified. The numerical simulation method is one of the most widely used methods in this field, but the application of this method in the new type of foundation is still based on existing experience. At present, there is no model test and study to testify whether the FE method can be used in the study of SPBF. This paper makes a breakthrough in proofing the applicability of FE method on SPBF through small-scale model tests. Based on the verified FE method, a series of bearing modes, bearing capacities and failure modes are analyzed, and the bearing characteristics of SPBF in saturated clay under vertical- and horizontal–moment loads are obtained, and provide a scientific support for the design and optimization of SPBF in practical engineering.

2. Materials and Methods

2.1. Description of Model Test

In order to verify the correctness of the current FE method, the indoor small-scale model tests were carried out according to the actual engineering prototype and the geometric similarity ratio is 1:40. The prototype is a 3.3 MW SPBF structure in Jilin, China.

The diameter of the prototype upper pile cap is 14 m and the height is 3.5 m, the outer diameter of the lower bucket is 14 m and the height is 12.5 m, the diameter of a pile is 0.8 m, and there are 70 piles in total. During the model design stage, the shape of the lower bucket skirt formed by secant piles of SPBF in actual engineering projects is complicated, and it produces challenges in the fabrication accuracy of the model to reproduce the structural characteristics of the engineering prototype foundation. At the initial stage of the small-scale model test, the purpose of scaling is only to perform some regularity studies of the SPBF and verify the applicability of FE method, rather than to simulate the actual problem exactly, since the soil cannot be scaled [30]. Therefore, the simplified homogeneous bucket skirt and pile cap with 45-gauge steel were adopted to simulate the actual structure. The schematic and the detailed dimensions of the bucket foundation model are shown in Figure 4 and Table 1.

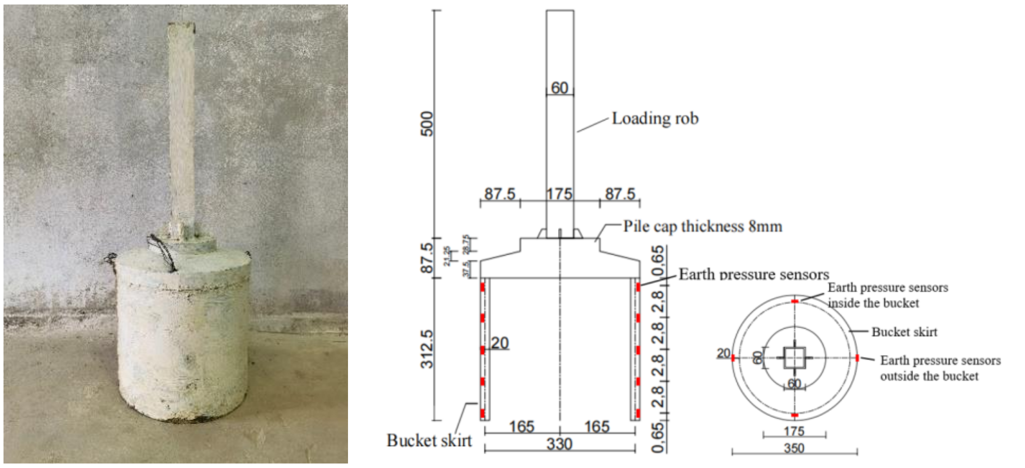

(a) (b)

Figure 4. The SPBF test model. (**a**) Test model. (**b**) Schematic of the model with dimensions (unit: mm).

Table 1. Dimensions of the experimental model and prototype foundation (unit: m).

	Pile Cap Diameter D_m	Pile Cap Height H_c	Bucket Height H_z	Bucket Thickness/ Pile Diameter T_z
Model	0.35	0.0875	0.3125	0.02
Prototype	14	3.5	12.5	0.8

The laboratory saturated clay is used to simulate the actual geological condition due to the high underground water level in the actual project. Details of the physical and mechanical properties of the saturated clay are listed in Table 2, considering that in saturated clay, the loading time of the wind turbine under extreme load is short and there is no time for drainage in the clay, which is an undrained condition. The in-situ undrained strength S_u of soil sample is shown in Table 3. Assuming that the undrained shear strength S_u of saturated clay increases linearly with the increase of depth, the undrained shear strength S_u is determined from:

$$S_u = S_{um} + kz \tag{1}$$

where S_{u0} is the undrained shear strength at depth z (kPa), S_{um} is the undrained shear strength of clay at the surface (kPa), z is the depth (m), and k is the growth coefficient of soil strength. The k value is the slope of the fitting curve of the undrained shear strength in different depths (see Figure 5). The k values in the vertical loading test and horizontal–moment loading test are −15 and −18, respectively.

Table 2. Physical and mechanical properties of the soil.

Soil	Water Content w (%)	Density ρ (g/cm^3)	Internal Friction φ (°)	Cohesion C (kPa)	Void Rate e	Compressive Modulus E_s (MPa)	Specific Gravity
Saturated clay	40.9	1.810	5.3	5	1.117	2.72	2.72

Table 3. Results of undrained shear strength S_u.

Depth, z (m)	Undrained Shear Strength of Vertical Loading Case, S_u (kPa)	Undrained Shear Strength of Horizontal-Moment Loading Case, S_u (kPa)
0.1	2	2
0.2	3	4
0.3	5	7
0.4	6	8
0.5	8	9
Avg	4.8	6

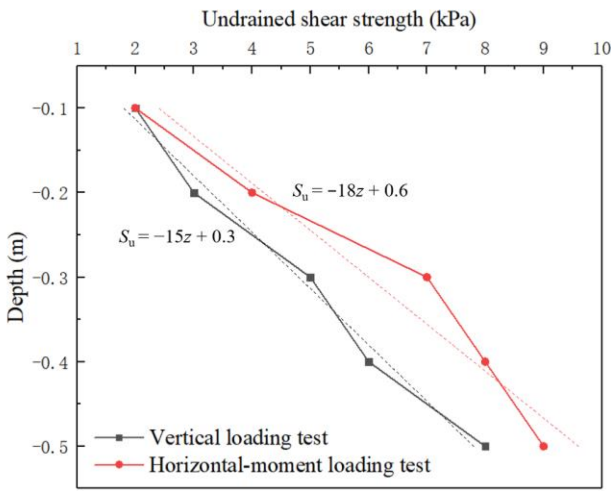

Figure 5. The undrained shear strength at different depths.

The loading hydraulic jacks were adopted in the tests to apply displacement, and the height of the horizontal loading point is 0.4 m above the top of the pile cap. The load of the bucket foundation model during the loading process was recorded by a load cell and the settlement/displacement of the bucket foundation model was recorded by a displacement sensor, while the earth pressures inside and outside the bucket wall at different depths were measured by several earth pressure sensors. The earth pressure sensors were arranged symmetrically in four rows with equal axial distance, there were 20 earth pressure sensors used in the tests, and a detailed layout of earth pressure sensors is shown in Figure 4b. Due to the long preparation period of clay, only two groups of tests were carried out in this research, namely, one vertical loading test and one horizontal–moment loading test.

2.2. Description of Numerical Models

2.2.1. Finite Element Model of Model Test

The FE model of the bucket foundation model is established according to the actual test model. The soil and lower bucket skirt are modeled using an eight-node brick element with reduced integration (C3D8R), and the loading rod and the pile cap are modeled using a four-node shell element with reduced integration (S4R) element type (as shown in Figure 6). According to the experimental loading conditions, a rigid loading rod is built on the top of the pile cap of the bucket foundation.

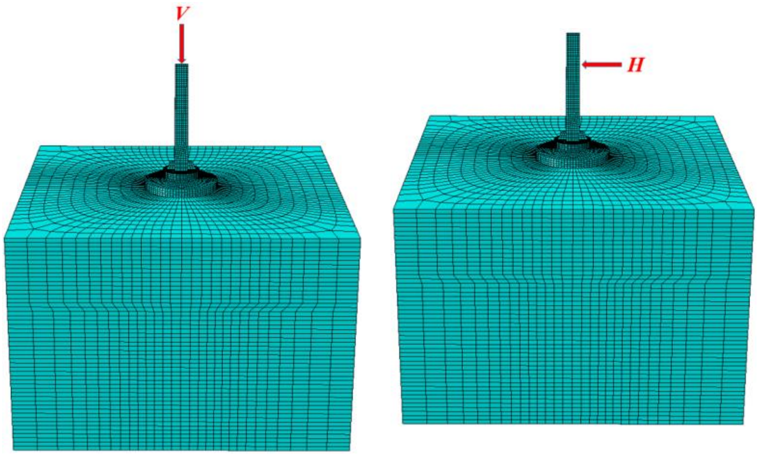

Figure 6. Loading states and FE models.

2.2.2. Finite Element Model of the Prototype

The FE model of the actual engineering prototype is established. The C3D8R element type is used to model the soil and the foundation, and the two-node truss element (T3D2) is used to model anchors and steel bars. In order to increase the accuracy of calculation, the mesh of the soil surrounding the SPBF model is relatively refined. The specific dimensions of SPBF have been described in Figure 2 and Section 2.1. The FE model is shown in Figure 7.

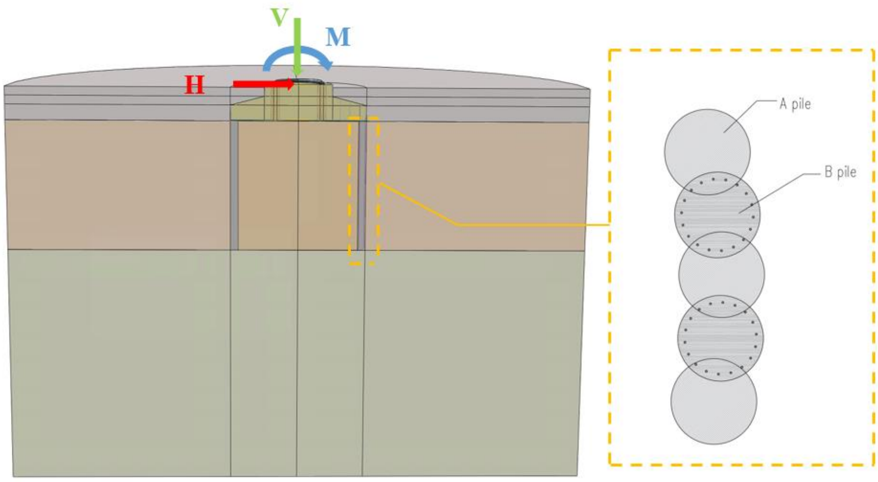

Figure 7. The FE model of SPBF.

2.2.3. Soil and Structure Properties

The soil-structure interaction (SSI) will affect the calculation result of bearing capacity [31–39]. To describe SSI, an ideal elastoplastic constitutive model based on Tresca failure criterion is used to simulate the normally consolidated clay [40,41]. The internal friction angle and dilation angle are set as 0 and the cohesion is equal to S_u in Mohr–Coulomb's model to adopt the Tresca failure criterion in ABAQUS. The Young's modulus E_u of soil under the undrained condition also increases linearly with the increase in depth, and combined with previous research results, the Young's modulus of clay generally ranges from 200 to 500 times the undrained shear strength [42–45]. Herein, the Young's modulus of clay is taken as 500 times the undrained shear strength in this research [46,47].

For the FE model of the small-scale model test, the linear elastic model is adopted to simulate the simplified homogeneous bucket skirt and pile cap with 45-gauge steel, and the elastic modulus and Poisson's ratio of bucket foundation model are 200 GPa and 0.3, respectively. Additionally, for the FE model of the prototype, the concrete damaged plasticity (CDP) model is adopted to simulate the C40 concrete pile cap and the C30 concrete bucket skirt, and the elastoplastic constitutive model is adopted to simulate the Q345E steel structures and HRB400 steel bars.

2.2.4. Boundary Condition and Contact

The surface-to-surface contact pair with an allowed finite sliding is applied to simulate the bucket–soil interface. The normal contact behavior between the bucket skirt and soil adopts the "hard" condition with no allowed separation after contact condition, while the tangential contact behavior is defined as "rough" contact condition to simulate the undrained behavior of clay [44,48,49].

For the FE model of model test, the displacement control method is adopted, which is widely used to calculate the bearing capacity of the bucket foundation in FE models [21,28,30]. Extract the displacement and load of the reference point, and draw them into the load–displacement curve, when the curve has an inflection point or reaches a certain displacement, it is determined that the foundation has reached its limit state. In the simulation of the vertical loading test, the displacement is coupling on the reference point at the center of the top of the rigid loading rod, while in the simulation of the horizontal–moment loading test, the horizontal displacement is coupled on the reference point on the side of the rigid loading rod that is located at the loading height of 0.4 m from the top of the pile cap. The loading states and FE models are shown in Figure 6. No displacement and rotation are adopted to the bottom boundary of soil (U1 = U2 = U3 = UR1 = UR2 = UR3 = 0), and horizontal displacement and vertical rotation are not allowed to the lateral boundary of soil (U1 = U2 = UR3 = 0).

In the analysis of the bearing mode, in order to clarify the bearing mode of the SPBF under the action of the composite load in the actual project, the engineering load is coupled on the reference point at the top of the flange. The F_{xy} = 894 kN, F_z = $-$4358.9 kN and M_{xy} = 99,672.06 kN·m, while in the analysis of the bearing capacity and failure mode, the distance between the loading point and the foundation can be calculated as 111.49 m through the horizontal and bending moment loads of the actual project [41]. The effect of horizontal–moment load on the foundation of the wind turbine is simulated by applying horizontal displacement at this reference point, and the failure load can be further predicted. Due to the symmetry, only half of the FE model is adopted in the bearing capacity and failure mode analysis, the displacement is vertical to the symmetry plane, and the rotation with the axis in the symmetry plane are not allowed (U2 = UR1 = UR3 = 0).

2.3. Validation of Finite Element Method

Figure 8 shows the comparison of bearing capacity between FE results and test results under the action of vertical load and horizontal–moment load, respectively. The vertical load firstly increases linearly with the increase of settlement. As the settlement of the bucket foundation model reaches about 0.02 m, an inflection point appears on the vertical load-settlement curve, and the growth rate of the vertical load begins to slow down. It indicates that the bucket foundation model reaches the ultimate state. After the settlement reaches the ultimate state, the bucket foundation model fails. In addition, the trend of the horizontal load–displacement curve is similar to that of the vertical load-settlement curve, and the bucket foundation model reaches the ultimate state when the displacement of the bucket foundation model reaches about 0.03 m.

The comparison results illustrate that the overall trends of FE results and test results are consistent. The deviation of vertical bearing capacity is 10.65%, while that of horizontal–moment bearing capacity is 10.25%. It is worthwhile to mention that the boundary conditions set in the FE models are reasonable, and the model tests can be accurately simulated by the FE method.

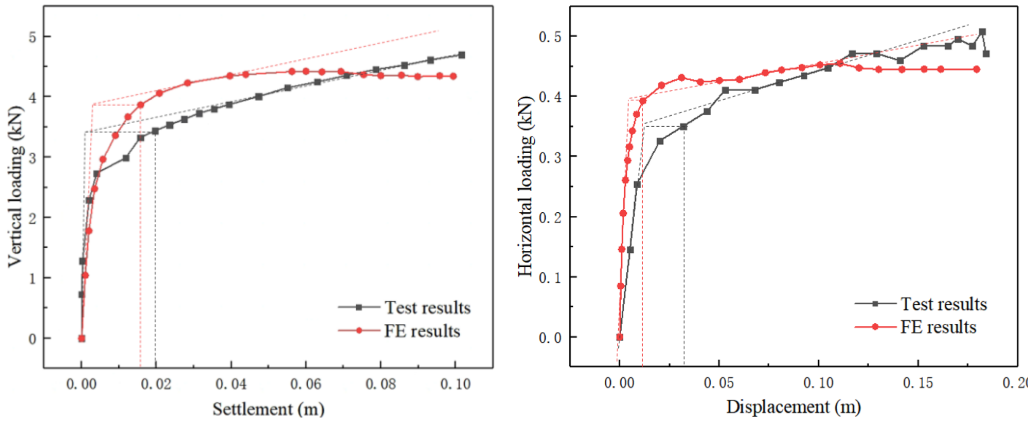

(**a**) (**b**)

Figure 8. Comparison of bearing capacity between FE results and test results. (**a**) The vertical load-settlement curves. (**b**) The horizontal load–displacement curves.

Figure 9 shows the comparison of earth pressure distribution curves between FE results and test results under the action of vertical load and horizontal–moment load, respectively. The comparison between FE results and test results indicates that the overall trends of earth pressure distribution curves under vertical load and horizontal–moment load are consistent. The comparison results prove that the boundary conditions applied in the FE models can accurately simulate the stress state of the bucket foundation model during the tests. In the results obtained by the FE method, the earth pressure results inside the bucket skirt in the vertical loading test are larger than that obtained in the model test, this is because the FE method is different from the actual situation in simulating soil extrusion. The same phenomenon that occurred in the bucket skirt tip under horizontal–moment load is also due to the same reason [50].

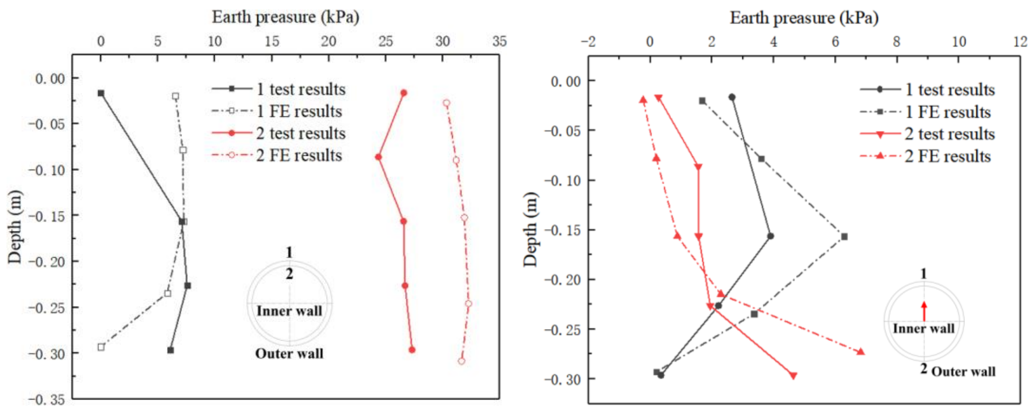

(**a**) (**b**)

Figure 9. Comparison of earth pressure distribution curves between FE results and test results. (**a**) The comparison of vertical loading test. (**b**) The comparison of horizontal–moment loading test.

From the above comparison results, the feasibility of the FE method adopted in this paper is fully proved. The conclusion demonstrates that the FE method can provide accurate results and reflect the true stress state of foundation and soil and can offer a reliable basis for SPBF design and safety evaluation in the future.

3. Results

3.1. Bearing Mode of SPBF

The displacement contour and displacement vector diagram of the SPBF under the actual engineering load is shown in Figure 10. Compared with the bearing mode of the pile foundation, the obvious rotation center can be seen from the bearing mode of the prestressed tubular foundation. Therefore, from the perspective of the distribution of displacement, the bearing mode of SPBF is corresponding to that of the prestressed tubular foundation. In the future, the structural design and optimization of the SPBF should be based on the calculation method of the prestressed tubular foundation. Under the action of actual engineering load, the rotation center of the SPBF is located at the point approximately 0.64 times the bucket skirt height below the bottom of the pile cap. As the load continues to increase, the rotation center of the foundation will continue to move towards the center of the bucket skirt, and finally the SPBF will fail.

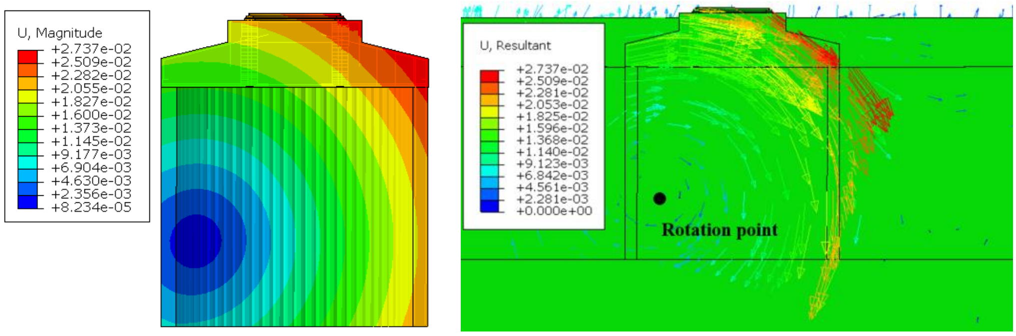

(**a**) (**b**)

Figure 10. FE results of SPBF under actual engineering load. (**a**) Displacement contour. (**b**) Displacement vector diagram.

3.2. Bearing Capacity of the SPBF

3.2.1. Vertical Bearing Capacity of the SPBF

The vertical load-settlement curve of the SPBF is shown in Figure 11. The result shows that the vertical bearing capacity of the SPBF is 96.53 meganewton (MN) with a settlement of 0.21 m. The vertical load of SPBF firstly increases with the increase of settlement, but after the settlement reaches 0.21 m, which is the ultimate state of SPBF, the vertical load on the SPBF drops rapidly. The ultimate settlement is twice of 0.1 m, which is the allowable settlement of the Code for Design of Wind Turbine Foundations for Onshore Wind Power Projects (NB/T 10311-2019), meaning that SPBF has twice the safety margin [26]. However, the ultimate settlement value has not reached 0.03 to 0.07 times the diameter of the bucket skirt, which is the settlement of foundation failure on soft soil for the gentle vertical load-settlement curve, proposed by Hesar [46] and Vesic [47]. In addition, the trend of the vertical load-settlement curve is different from the trend caused by the soil failure. The above analysis illustrates that the failure of the SPBF is caused by structural damage.

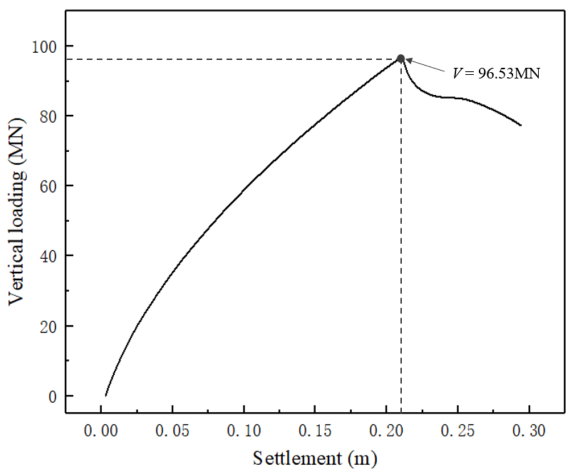

Figure 11. The vertical load-settlement curve of the SPBF.

From the displacement contour and displacement vector diagram (see Figure 12), the SPBF has an obvious settlement under the action of vertical load, and the soil inside the bucket skirt is significantly compressed. From Figure 13, the disengagement rate of SPBF is 3.19%. The disengagement area is distributed at the junction of the pile cap and the bucket skirt, and is caused by the deformation of the pile cap.

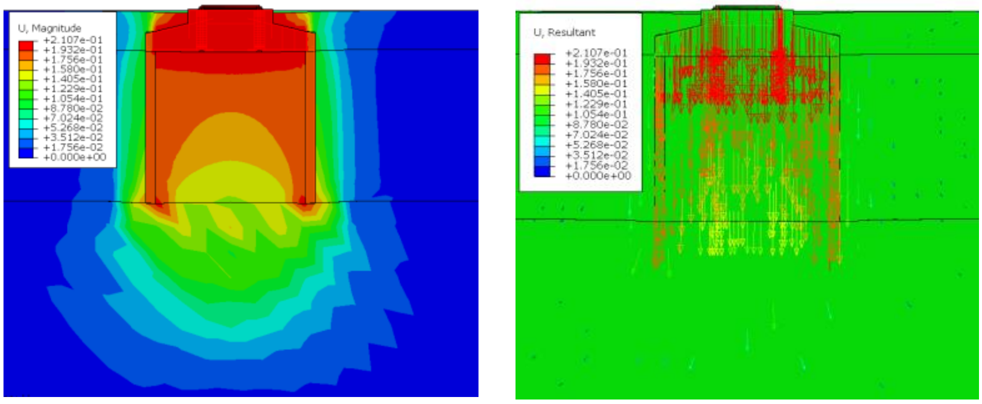

(**a**) (**b**)

Figure 12. Displacement of SPBF under vertical load. (**a**) Displacement contour. (**b**) Displacement vector diagram.

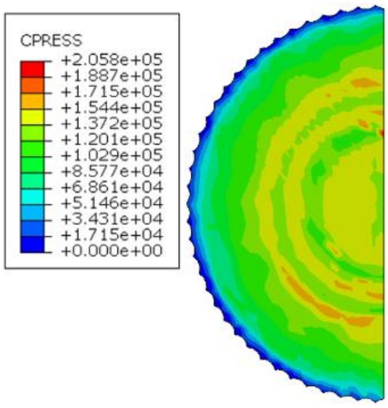

Figure 13. Soil pressure under the pile cap at the ultimate state.

In Figures 14 and 15, the upper load is transmitted to the pile cap through the flange, which causes the pile cap to receive a large, concentrated stress at this position, and the bucket skirt provides a larger reaction force to the pile cap, resulting in the concrete of the pile cap reaching its tensile strength and compressive strength. Eventually, the failure areas run through the entire pile cap, and the SPBF structure reaches the ultimate state and fails. The result is that the concrete of the pile cap is the weak part of SPBF under the vertical load.

3.2.2. Horizontal Bearing Capacity of the SPBF

The horizontal load–displacement curve of the SPBF is shown in Figure 16. The result shows that the horizontal–moment bearing capacity of the SPBF is 1.62 MN with a displacement of 0.50 m. The trend of the horizontal load–displacement curve is similar to the trend of curve of the horizontal–moment loading test in Section 2.3.

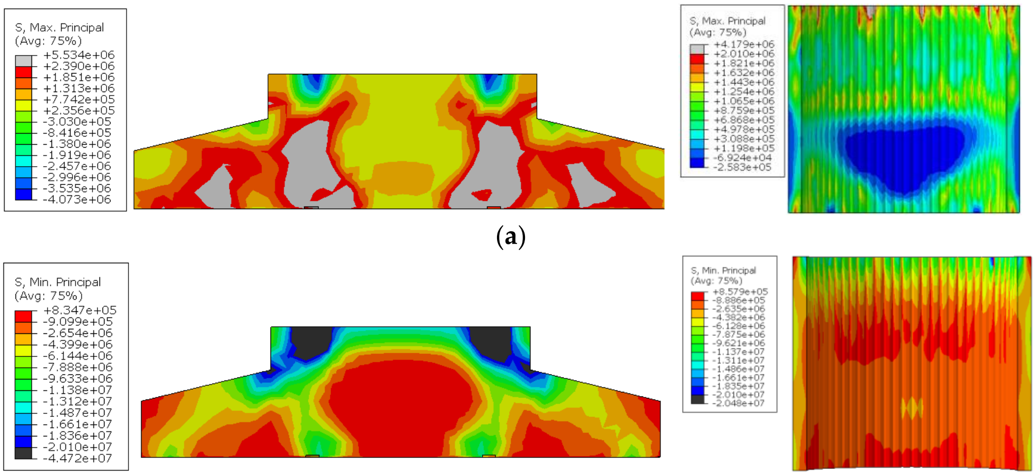

(**a**)

(**b**)

Figure 14. The stress contours of SPBF under vertical load. (**a**) Max. principal stress contour of SPBF. (**b**) Min. principal stress contour of concrete.

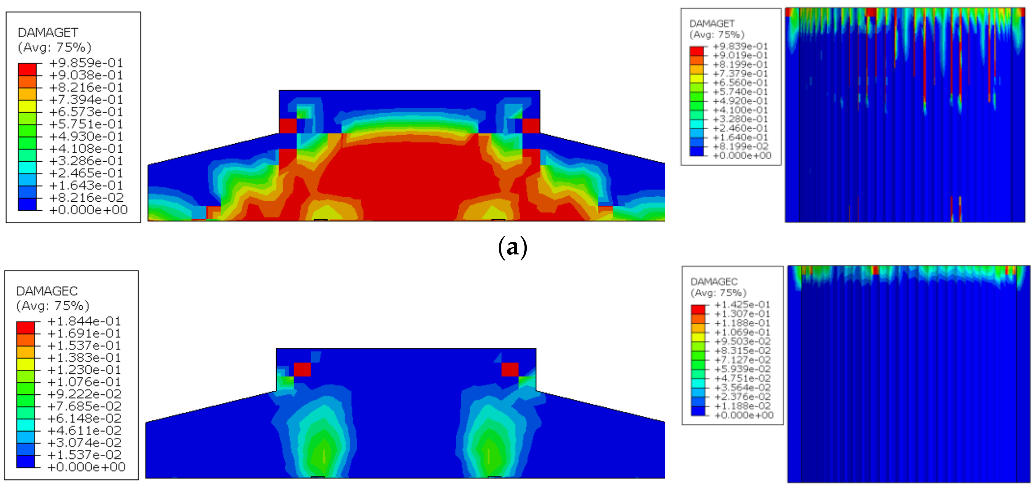

(**a**)

(**b**)

Figure 15. The damage contours of SPBF under vertical load. (**a**) DAMAGET contour of SPBF. (**b**) DAMAGEC contour of concrete.

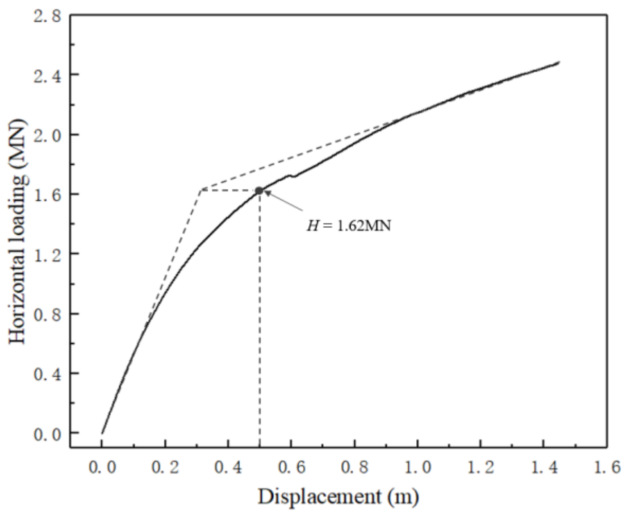

Figure 16. The horizontal load–displacement curve of the SPBF.

The displacement of SPBF under horizontal load at the ultimate state is shown in Figure 17. From the displacement contour and displacement vector diagram, the SPBF has an obvious rotation point under the action of horizontal–moment load, and the rotation point of the SPBF is located at the point approximately 0.72 times the bucket skirt height below the bottom of the pile cap, while the bottom disengagement rate of SPBF is 8.35% (see Figure 18). The FE results of the displacement contour and displacement vector diagram illustrate that the bearing mode of SPBF is similar to that of the prestressed tubular foundation, which is in further support of the hypothesis proposed in Section 1. Therefore, the following analysis will be expanded with reference to the standard of the prestressed tubular foundation.

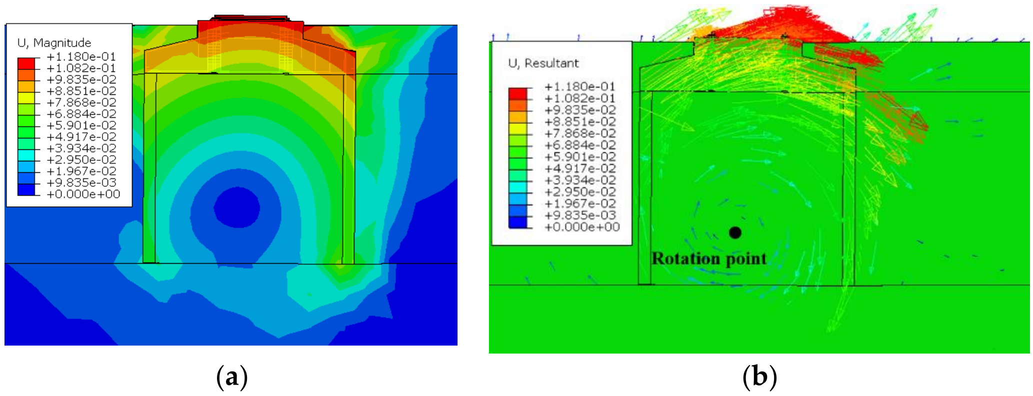

Figure 17. Displacement of SPBF under horizontal–moment load. (**a**) Displacement contour. (**b**) Displacement vector diagram.

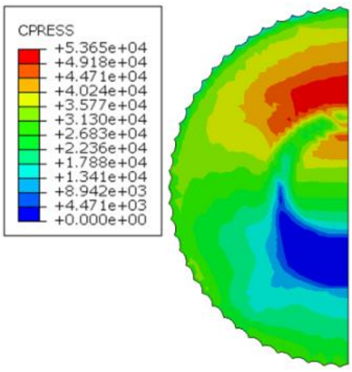

Figure 18. Soil pressure under the pile cap.

From the results illustrated in Figure 19, the inclination rate of the top of flange and the bottom of the pile cap are 4.16‰ and 3.21‰, respectively. The inclination rate of the flange top is larger than 4‰, which is the specified inclination rate of prestressed tubular foundation proposed in the Code for Design of Wind Turbine Foundations for Onshore Wind Power Projects (NB/T 10311-2019), while that of the bottom of the pile cap has not reached the specified value [8]. Combined with the results illustrated in Figure 20, the failure of the SPBF is caused by part of anchor bolts of the pile cap reaching the tensile strength, which are close to the loading force. It is precisely that of the yield of the anchor bolts, resulting in the inclination rate of the flange top exceeding the specified value.

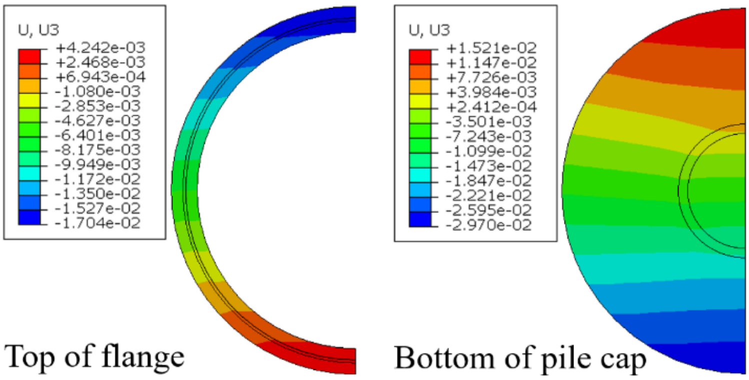

Figure 19. Displacement contour of flange top and pile cap bottom.

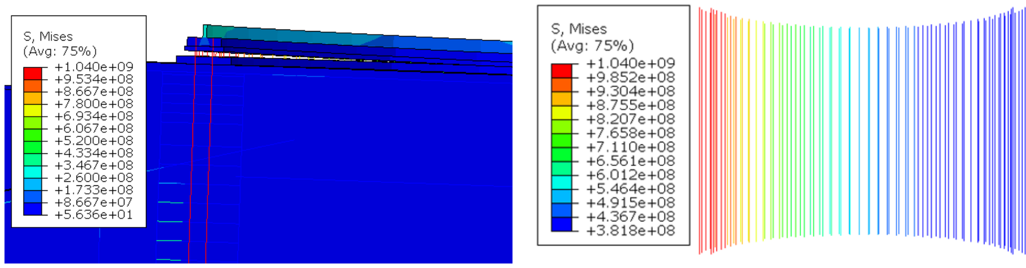

Figure 20. Mises stress contours of steel at the ultimate state (5 times deformation).

Meanwhile, the stress contours and the damage contours of SPBF are presented in Figures 21 and 22. The results show that the concrete of the pile cap and bucket skirt at the ultimate state exceed its standard value slightly, and the area of tensile damaged concrete is developed deep into the pile cap but has not penetrated yet. The concrete surrounding the failed anchor bolts of the pile cap is damaged due to excessive compression, resulting in the disengagement between the pile cap bottom and soil (see Figure 17). The results illustrate that the anchor bolts are the weak part of SPBF under the horizontal–moment load.

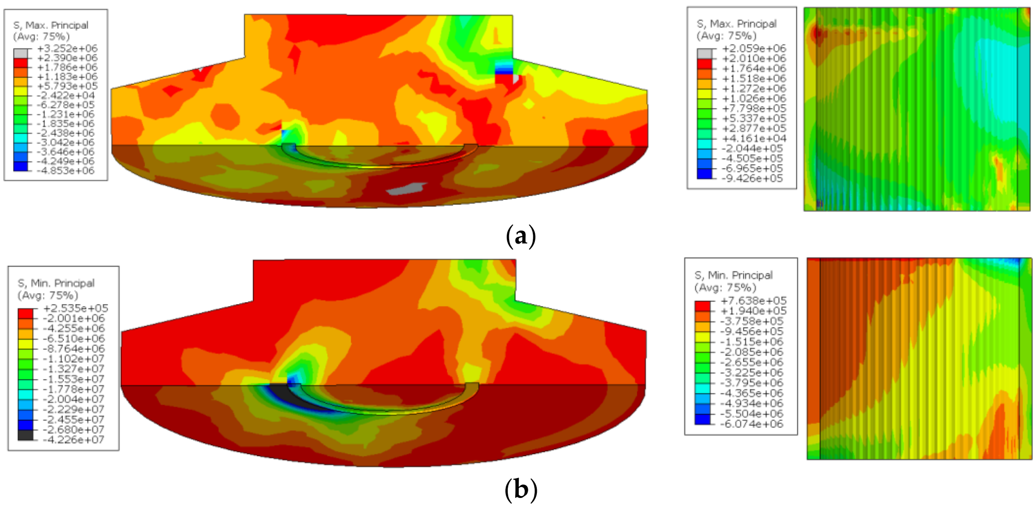

Figure 21. The stress contours of SPBF under horizontal load. (**a**) Max. principal stress contour of SPBF. (**b**) Min. principal stress contour of concrete.

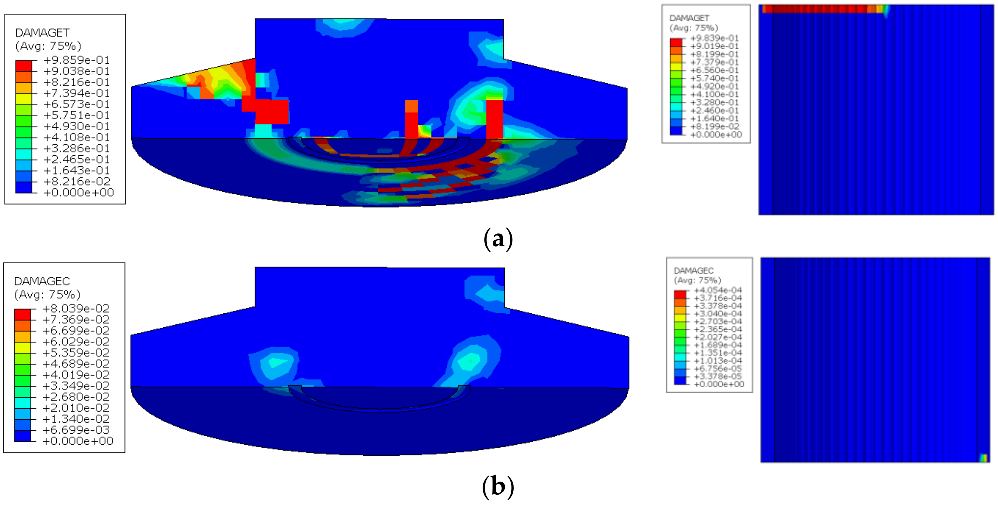

Figure 22. The damage contours of SPBF under horizontal load. (**a**) DAMAGET contour of SPBF. (**b**) DAMAGEC contour of concrete.

4. Discussion

This paper firstly introduces the innovative SPBF that has been applied in practical engineering and its advantages in the introduction. However, in order to further study the bearing performance of the SPBF, the bearing mode, bearing capacity and failure mode of the new type of foundation structure are questioned, and whether the current FE method used to explore the above problems is applicable is not clear. Therefore, a validation study of the FE method is carried out through laboratory-scale model tests, and the applicability of the FE method was proved. Finally, after a series of numerical simulations, a series of conclusions about the bearing characteristics of the foundation are obtained.

However, the research in this paper is only carried out in saturated clay, and the bearing characteristics of the SPBF under other geological conditions needs further analysis and research. In actual engineering, the loads acting on the foundation are more complex, and in most cases, the foundation is affected by composite loads, which needs further consideration. In addition, the foundation has a large safety margin, indicating that the foundation design is conservative and has optimization space. Meanwhile, this paper only considers the force of the entire bucket skirt, but the force of a single pile is also very important and we need to conduct in-depth research on this issue in the future. The sensitivity factor analysis of the bearing capacity can be carried out in the next study and will a provide theoretical basis and scientific guidance for the structural optimization design of the SPBF in the future.

5. Conclusions

In this paper, the innovative secant piled-bucket foundation (SPBF) has been intensively studied, which is creatively proposed for onshore wind projects to adapt to the trend of large-capacity wind turbines. The comparison with the pile foundation under the same conditions shows that the SPBF has certain significance for the development of the wind power industry. Therefore, this paper conducts further research on the foundation. Small-scale model tests and FE analysis of SPBF in saturated clay are carried out. The characteristics of the bearing capacity and performances of SPBF under various loads are investigated. The following main conclusions can be drawn:

(1) The FE method is validated by the model tests. The deviation of vertical bearing capacity is 10.65%, while that of horizontal–moment bearing capacity is 10.25%. The overall trends of earth pressure distribution curves under vertical load and horizontal–moment load of FE results and test results are consistent.
(2) According to the FE analysis results of the SPBF prototype in saturated clay, the bearing mode of the SPBF is clear. The bearing mode of SPBF under the actual

engineering load is corresponding to the prestressed tubular foundation. There is an obvious rotation center of the SPBF, which is located at the point approximately 0.64 times the bucket skirt height below the bottom of the pile cap. Moreover, the bearing mode of SPBF is further proved in the following research about the bearing performances of SPBF. In the design and further optimization of SPBF in the future, the standard of the prestressed tubular foundation can be referred to.

(3) The bearing capacity and failure mode analysis of SPBF in engineering scales under different loads are carried out by the FE method. The vertical bearing capacity of SPBF is 96.53 MN with a settlement of 0.21 m, and the failure of SPBF is caused by the concrete cracking of the pile cap, while the horizontal–moment bearing capacity of SPBF is 1.62 MN with a displacement of 0.50 m and the failure of SPBF is caused by the yielding of the anchor bolts. Compared with the actual engineering load, it has a large safety margin, which can be further optimized in the future.

The above conclusions show that in actual engineering applications, although the SPBF has great economic advantages compared with the traditional pile foundation, the current design of the new infrastructure is still conservative and has a lot of room for optimization. In the future, if the SPBF is applied in mass production, the construction cost and floor area of the wind turbine can be significantly reduced. It is estimated that after the optimization of the structure, about 20% of the fans can be added under the same amount of work and land occupation, which can greatly promote the development of the wind power market. Through the analysis and research in this paper, it is found that SPBF has broad application prospects and is worth further promotion and research.

Author Contributions: Conceptualization, H.W. and Y.X.; methodology, H.W., Y.X. and X.Y.; validation, Y.X.; investigation, H.W., Y.G., L.Z., M.D. and H.J.; resources, H.W., Y.G., L.Z., M.D. and H.J.; data curation, Y.X.; writing—original draft preparation, H.W. and Y.X.; writing—review and editing, Y.G. and X.Y.; supervision, H.W. All authors have read and agreed to the published version of the manuscript.

Funding: This research received no external funding.

Institutional Review Board Statement: Not applicable.

Informed Consent Statement: Not applicable.

Data Availability Statement: Not applicable.

Acknowledgments: The authors acknowledge support from China Huaneng Clean Energy Research Institute.

Conflicts of Interest: The authors declare no conflict of interest.

References

1. Yang, J.; Liu, Q.; Li, X.; Cui, X. Overview of Wind Power in China: Status and Future. *Sustainability* **2017**, *9*, 1454. [CrossRef]
2. Wang, B.; Yuan, M.-H.; Li, L.; Yuan, C.-F.; Li, Y.; Shen, K.-M. Sensitivity Analysis of Factors Affecting the Bearing Capacity of Suction Bucket Foundation in Soft Clay. *Sustainability* **2022**, *14*, 9615. [CrossRef]
3. Liu, M.; Lian, J.; Yang, M. Experimental and numerical studies on lateral bearing capacity of bucket foundation in saturated sand. *Ocean Eng.* **2017**, *144*, 14–20. [CrossRef]
4. Iskander, M.; El-Gharbawy, S.; Olson, R. Performance of suction caissons in sand and clay. *Can. Geotech. J.* **2002**, *39*, 576–584. [CrossRef]
5. Tran, M.N.; Randolph, M.F.; Airey, D.W. Installation of suction caissons in sand with silt layers. *J. Geotech. Geoenviron. Eng.* **2007**, *133*, 1183–1191. [CrossRef]
6. Zhu, B.; Kong, D.-Q.; Chen, R.-P.; Kong, L.-G.; Chen, Y.-M. Installation and lateral loading tests of suction caissons in silt. *Can. Geotech. J.* **2011**, *48*, 1070–1084. [CrossRef]
7. Zhang, L.; Wei, Z.; Ma, Z.; Ye, J.; Guo, N.; Hao, H.; Jiang, H.; Li, J. Bucket Foundation Structure and Wind Turbine for Collapsible Loess Area. Utility Model Patent CN216428321U, 3 May 2022.
8. Institute CREE. *Code for Design of Wind Turbine Foundations for Onshore Wind Power Projects*; China Water & Power Press: Beijing, China, 2020.

9. Ding, H.; Liu, Y.; Zhang, P.; Le, C. Model tests on the bearing capacity of wide-shallow composite bucket foundations for offshore wind turbines in clay. *Ocean Eng.* **2015**, *103*, 114–122. [CrossRef]
10. Zhu, B.; Zhang, W.-L.; Ying, P.-P.; Chen, Y.-M. Deflection-Based Bearing Capacity of Suction Caisson Foundations of Offshore Wind Turbines. *J. Geotech. Geoenviron. Eng.* **2014**, *140*, 04014013. [CrossRef]
11. Guo, Y.; Zhang, P.; Ding, H.; Le, C. Experimental Study on Torsion Resistance of Foundation Ring Land-Based Wind Power Expanded Foundation Scale Model. *Appl. Sci.* **2020**, *10*, 5612. [CrossRef]
12. Zhao, B.; Gao, H.; Wang, Z.; Lu, Z. Shaking table test on vibration control effects of a monopile offshore wind turbine with a tuned mass damper. *Wind Energy* **2018**, *21*, 1309–1328. [CrossRef]
13. Zachert, H.; Wichtmann, T.; Kudella, P.; Triantafyllidis, T. Inspection of a high-cycle accumulation model for sand based on recalculations of a full-scale test on a gravity base foundation for offshore wind turbines. *Comput. Geotech.* **2020**, *126*, 103727. [CrossRef]
14. Urban, S.; Strauss, A.; Schuetz, R.; Bergmeister, K.; Dehlinger, C. Dynamically loaded concrete structures—Monitoring-based assessment of the real degree of fatigue deterioration. *Struct. Concr.* **2014**, *15*, 530–542. [CrossRef]
15. He, M.; Bai, X.; Ma, R.; Huang, D. Structural monitoring of an onshore wind turbine foundation using strain sensors. *Struct. Infrastruct. Eng.* **2019**, *15*, 314–333. [CrossRef]
16. Urban, S.; Strauss, A.; Wagner, R.; Reiterer, M.; Dehlinger, C. Experimental modelling of fatigue processes to detect the real degree of deterioration Conceptual design of the fatigue tests at the Strabag-Gravity base in Cuxhaven. *Beton Stahlbetonbau* **2012**, *107*, 463–475. [CrossRef]
17. Vicent, S.; Kim, S.-R.; Hung, L.C. Evaluation of horizontal and vertical bearing capacities of offshore bucket work platforms in sand. *Appl. Ocean Res.* **2020**, *101*, 102198. [CrossRef]
18. Zhou, N.; Kou, H.-L.; Chen, Q. Horizontal cyclic response of bucket caisson for offshore wind turbines in over-consolidated clay. *Appl. Ocean Res.* **2022**, *118*, 102973. [CrossRef]
19. Ibsen, L.B.; Larsen, K.A.; Barari, A. Calibration of Failure Criteria for Bucket Foundations on Drained Sand under General Loading. *J. Geotech. Geoenviron. Eng.* **2014**, *140*. [CrossRef]
20. Kim, J.-H.; Jeong, Y.-H.; Kim, D.-S. Improved load capacity of a hybrid bucket foundation for offshore structures in sand. *Appl. Ocean Res.* **2020**, *101*, 102197. [CrossRef]
21. Li, J.; Guo, Y.; Lian, J.; Wang, H. Scour effects on the bearing capacity of multi-bucket jacket foundation for offshore wind turbines. *Ocean Eng.* **2022**, *259*, 111848. [CrossRef]
22. Liu, M.; Yang, M.; Wang, H. Bearing behavior of wide-shallow bucket foundation for offshore wind turbines in drained silty sand. *Ocean Eng.* **2014**, *82*, 169–179. [CrossRef]
23. Wang, G.; Gan, Y.; Le, C.; Yan, R.; Hu, X. Bearing Characteristics of Tripod Bucket Jacket Foundation for Offshore Wind Turbines in Sand under Monotonic Loads. *J. Mar. Sci. Eng.* **2022**, *10*, 199. [CrossRef]
24. Fan, K.-F.; Xun, Z.; Li, W.-X.; Wang, Q.-Q.; Yi, T. Horizontal bearing capacity of composite bucket foundation in clay: A case study. *Eng. Fail. Anal.* **2022**, *140*, 106572. [CrossRef]
25. Ding, H.; Hu, R.; Zhang, P.; Le, C. Load bearing behaviors of composite bucket foundations for offshore wind turbines on layered soil under combined loading. *Ocean Eng.* **2020**, *198*, 106997. [CrossRef]
26. Liu, R.; Yuan, Y.; Fu, D.; Sun, G. Numerical investigation to the cyclic loading effect on capacities of the offshore embedded circular foundation in clay. *Appl. Ocean Res.* **2022**, *119*, 103022. [CrossRef]
27. Jia, N.; Zhang, P.; Liu, Y.; Ding, H. Bearing capacity of composite bucket foundations for offshore wind turbines in silty sand. *Ocean Eng.* **2018**, *151*, 1–11. [CrossRef]
28. Wang, X.; Li, S.; Li, J. Load bearing mechanism and simplified design method of hybrid monopile foundation for offshore wind turbines. *Appl. Ocean Res.* **2022**, *126*, 103286. [CrossRef]
29. Xia, H.; Zhou, M.; Niu, F.; Zhang, X.; Tian, Y. Combined bearing capacity of bucket foundations in soft-over-stiff clay. *Appl. Ocean Res.* **2022**, *126*, 103299. [CrossRef]
30. Qian, J.; Mu, L.; Zhang, Y.; Zhang, Y. Behavior of a Structured Piled Beam-Slab Foundation for a Wind Turbine under Multidirectional Loads in Sand. *Int. J. Geomech.* **2021**, *21*, 04020267. [CrossRef]
31. Guo, Y.; Zhang, P.; Ding, H.; Le, C. Design and verification of the loading system and boundary conditions for wind turbine foundation model experiment. *Renew. Energy* **2021**, *172*, 16–33. [CrossRef]
32. Versteijlen, W.G.; Metrikine, A.V.; van Dalen, K.N. A method for identification of an effective Winkler foundation for large diameter offshore wind turbine support structures based on in-situ measured small-strain soil response and 3D modelling. *Eng. Struct.* **2016**, *124*, 221–236. [CrossRef]
33. Gourvenec, S. Shape effects on the capacity of rectangular footings under general loading. *Geotechnique* **2007**, *57*, 637–646. [CrossRef]
34. Kourkoulis, R.S.; Lekkakis, P.C.; Gelagoti, F.M.; Kaynia, A.M. Suction caisson foundations for offshore wind turbines subjected to wave and earthquake loading: Effect of soil-foundation interface. *Geotechnique* **2014**, *64*, 171–185. [CrossRef]
35. Shen, Z.; Feng, X.; Gourvenec, S. Undrained capacity of surface foundations with zero-tension interface under planar V-H-M loading. *Comput. Geotech.* **2016**, *73*, 47–57. [CrossRef]
36. Vulpe, C. Design method for the undrained capacity of skirted circular foundations under combined loading: Effect of deformable soil plug. *Geotechnique* **2015**, *65*, 669–683. [CrossRef]

37. Plodpradit, P.; Kwon, O.; Dinh, V.N.; Murphy, J.; Kim, K.-D. Suction Bucket Pile-Soil-Structure Interactions of Offshore Wind Turbine Jacket Foundations Using Coupled Dynamic Analysis. *J. Mar. Sci. Eng.* **2020**, *8*, 416. [CrossRef]
38. Li, J.; Lian, J.; Guo, Y.; Wang, H.; Yang, X. Numerical study on scour protection effect of monopile foundation based on disturbance structure. *Ocean Eng.* **2022**, *248*, 110856. [CrossRef]
39. Lian, J.; Li, J.; Guo, Y.; Wang, H.; Yang, X. Numerical study on local scour characteristics of multi-bucket jacket foundation considering exposed height. *Appl. Ocean Res.* **2022**, *121*, 103092. [CrossRef]
40. Xiao, Z.; Fu, D.; Zhou, Z.; Lu, Y.; Yan, Y. Effects of strain softening on the penetration resistance of offshore bucket foundation in nonhomogeneous clay. *Ocean Eng.* **2019**, *193*, 106594. [CrossRef]
41. Wang, J.; Sun, G.; Chen, G.; Yang, X. Finite element analyses of improved lateral performance of monopile when combined with bucket foundation for offshore wind turbines. *Appl. Ocean Res.* **2021**, *111*, 102647. [CrossRef]
42. Houlsby, G.T.; Martin, C.M. Undrained bearing capacity factors for conical footings on clay. *Geotechnique* **2003**, *53*, 513–520. [CrossRef]
43. Kim, S.-R.; Hung, L.C.; Oh, M. Group effect on bearing capacities of tripod bucket foundations in undrained clay. *Ocean Eng.* **2014**, *79*, 1–9. [CrossRef]
44. Fu, D.; Gaudin, C.; Tian, Y.; Cassidy, M.J.; Bienen, B. Uniaxial Capacities of Skirted Circular Foundations in Clay. *J. Geotech. Geoenviron. Eng.* **2017**, *143*, 04017022. [CrossRef]
45. Martin, C.M. Vertical bearing capacity of skirted circular foundations on Tresca soil. In Proceedings of the 15th International Conference on Soil Mechanics and Geotechnical Engineering, Istanbul, Turkey, 27–31 August 2001; pp. 743–746.
46. Mehravar, M.; Harireche, O.; Faramarzi, A. Evaluation of undrained failure envelopes of caisson foundations under combined loading. *Appl. Ocean Res.* **2016**, *59*, 129–137. [CrossRef]
47. Hung, L.C.; Kim, S.-R. Evaluation of Undrained Bearing Capacities of Bucket Foundations Under Combined Loads. *Mar. Georesour. Geotechnol.* **2014**, *32*, 76–92. [CrossRef]
48. Vulpe, C.; Gourvenec, S.; Leman, B.; Fung, K.N. Failure Envelope Approach for Consolidated Undrained Capacity of Shallow Foundations. *J. Geotech. Geoenviron. Eng.* **2016**, *142*. [CrossRef]
49. Vulpe, C.; Gourvenec, S.; Power, M. A generalised failure envelope for undrained capacity of circular shallow foundations under general loading. *Geotech. Lett.* **2014**, *4*, 187–196. [CrossRef]
50. Liu, M. Bearing Capacity and Optimization Design of Composite Bucket Foundation for Offshore Wind Turbine. Ph.D. Thesis, Tianjin University, Tianjin, China, 2014.